Journal of Inorganic and General Chemistry
ZAAC
Zeitschrift für anorganische und allgemeine Chemie
DOI: 10.1002/zaac.202000276
ARTICLE

Variability in the Formation and Framework Polymorphism of Metal-organic Frameworks based on Yttrium(III) and the Bifunctional Organic Linker 2,5-Dihydroxyterephthalic Acid

Pascal D. C. Dietzel,*[a] Richard Blom,[b] and Helmer Fjellvåg[c]

Abstract. Depending on the solvothermal reaction conditions, we obtained three different metal-organic frameworks with yttrium(III) as metal component and 2,5-dihdyroxyterepthalic acid (H_4dhtp) as bifunctional organic linker: $Y_2(H_2dhtp)_3(dmf)_4{\cdot}(dmf)_2$ (CPO-29) contains dinuclear, paddle-wheel like inorganic secondary building units (SBUs) connected by the organic linker to a network with α-Po topology, while $Y_2(H_2dhtp)(dhtp)(dmf)_2$ (CPO-30) and $Y_2(H_2dhtp)(dhtp)(dmf)_2(H_2O)_2{\cdot}(H_2O)_4$ (CPO-31) contain one-dimensional inorganic SBUs that differ in how the half- and fully deprotonated ligands are connected to and arranged around them. Only the carboxylic acid groups of the organic linker are deprotonated in CPO-29, while CPO-30 and CPO-31 contain both 2,5-dihydroxyterephthalate (H_2dhtp^{2-}) linkers and fully deprotonated 2,5-dioxidoterephthalate ($dhtp^{4-}$) linkers. All three compounds contain large volumes filled with solvent, but we were able to demonstrate permanence of porosity only for CPO-30. Variable temperature powder X-ray diffraction reveals that CPO-29 and CPO-31 undergo discontinuous phase transitions upon heating, and the flexibility of the framework structure indicated by these might be the reason for the inability to access the pore volume. Desolvated CPO-30 and CPO-31 are polymorphs, whose network structures differ in whether the H_2dhtp^{2-} and $dhtp^{4-}$ linkers are located in *cis* or *trans* arrangement around the inorganic SBU.

Introduction

There is significant research interest on metal-organic frameworks (MOFs) due to their immense potential in areas of practical importance like gas sorption and separation, sensor systems and catalysis.[1] On a fundamental level, they continue to intrigue because of the diversity of framework structures,[2] which is a natural result of the countless possible combinations of inorganic and organic building blocks that can be used to construct the framework. Consequently, it is still possible to discover surprising and fascinating new ways of assembling secondary building units. In particular, utilization of larger ions with higher coordination numbers is expected to lead to more variation in metal coordination environments and the way framework structures are constructed for a given organic ligand, and higher charged metal ions might lead to stronger coordination bonds and hence more stable frameworks and/or larger inorganic oxo-cluster building units not observed for MOFs based on divalent cations.[3]

2,5-Dihydroxyterephthalic acid (H_4dhtp) is a versatile bifunctional organic linker that can employ a large variety of coordination modes. In accordance with the different acidity of its functional groups, it can connect to a metal ion either exclusively through the carboxylate group, or additionally through the oxygen atom of the hydroxyl group. The first mode, with network connectivity established only through the carboxylate groups, has been first encountered in the non-porous $Zn(H_2dhtp)(H_2O)_2$[4] and the copper compound Cu(tmen)(H_2dhtp),[5] which contain one-dimensional zigzag chains, the non-porous three-dimensional network compound $Mg(H_2dhtp)(H_2O)_2$ (CPO-26-Mg, CPO: Coordination Polymer of Oslo),[6] and the porous $Sc_3O(H_2dhtp)_3X{\cdot}x$DEF (CPO-28)[7] whose structure is analogous to the MIL-88 type compounds[8] and contains trimers of scandium octahedra connected through a common μ_3-O oxygen atom. Subsequently, several more alkaline earth and lanthanide based MOFs with this coordination mode were reported.[9] The second mode, utilizing all functional groups in network construction, is found most prominently in the porous honeycomb analogous compounds $M_2(dhtp)(H_2O){\cdot}8H_2O$ (CPO-27-M, also known as M-MOF-74 or M_2(dobdc), M = Mg, Mn, Fe, Co, Ni, Cu, Zn),[6,10] which are of particular interest because the high concentrations of coordinatively unsaturated metal sites in the activated materials impart favorable properties as sorbents, even for gases with pronounced difference in chemical properties as hydrogen[10c,10e,11] and carbon dioxide.[12] The hydroxyl group is usually deprotonated, as in CPO-27, when involved in framework construction. However, there are examples of non-deprotonated hydroxyl groups that participate in network con-

* Prof. Dr. P. D. C. Dietzel
E-mail: pascal.dietzel@uib.no
[a] Department of Chemistry
University of Bergen
P.O.box 7803, 5020 Bergen, Norway
[b] SINTEF Industry
Postboks 124 Blindern, 0314 Oslo, Norway
[c] Centre for Materials Science and Nanotechnology and Department of Chemistry
University of Oslo
Postboks 1033 Blindern, 0315 Oslo, Norway
Supporting information for this article is available on the WWW under **http://dx.doi.org/10.1002/zaac.202000276** or from the author.

struction with structurally related hydroxyl/carboxylic acid linkers.[13]

Herein, we extend our previous work on exploring the structural chemistry of coordination polymers formed by 2,5-dihydroxyterephthalic acid and divalent alkaline earth and transition metal ions and trivalent scandium towards the larger yttrium ion. Calcium and yttrium share a diagonal relationship in the periodic table of elements. Both typically employ coordination numbers above 6, which results in a high degree of flexibility of connectivity in framework construction. In the case of calcium, several different crystal structures have been observed with 2,5-dihydroxyterephthalate as linker.[9a–9c] Yttrium and lanthanide compounds are often isostructural, and the Y compounds can usually be doped easily with lanthanides. Thus, yttrium-organic frameworks have potential as host material to take advantage of the optical and magnetic properties of suitable lanthanide ions. Prior to investigations in this direction, potential host materials must be identified and characterized. Here, we report the formation of three metal-organic frameworks from yttrium and H_4dhtp, depending on reaction conditions. Their crystal structures are described and compared. Of particular interest is that two of the frameworks are polymorphs, whose framework structure differs by the position of fully and partially deprotonated linker molecule in respect to each other. All three compounds contain large volumes occupied by solvent molecules and potentially accessible coordination sites at the yttrium ion. The compounds were investigated in respect to their thermal stability by thermogravimetry and variable temperature powder X-ray diffraction. Collapse of the crystalline framework occurs often at lower temperatures than suggested by the onset of the weight loss which indicates decomposition of the compound. The combination of these two experimental techniques allows distinguishing between apparent thermal stability of the desolvated compound and the actual collapse of the framework to an amorphous compound as represented by the loss of crystallinity of the sample.

Experimental Section

All chemicals were commercially available and used as received. The purity of the bulk samples was confirmed by comparison of the powder X-ray diffraction patterns collected on a Siemens D5000 diffractometer and the calculated pattern based on the single crystal structure solution (Figures S2 and S3, Supporting Information). Thermogravimetric analyses were performed using a Perkin–Elmer TGA7 instrument. The samples were heated from room temperature to 600, 700, or 800 °C at a rate of 2 °C·min^{-1} in nitrogen atmosphere. Nitrogen gas adsorption at 77 K was measured using a BELSORP-miniII. IR spectra were recorded using a Nicolet iS50 instrument.

Synthesis of $Y_2(H_2dhtp)_3(dmf)_4\cdot(dmf)_2$ (CPO-29): A solid mixture of yttrium nitrate hexahydrate (0.257 g, 0.67 mmol) and 2,5-dihydroxyterephthalic acid (0.198 g, 1 mmol) was combined with *N*,*N*-dimethylformamide (12 mL) and water (1 mL) in a Teflon lined stainless steel autoclave and heated to 110 °C for 24 h. The reaction yielded large colorless crystals that were isolated by filtration. Yield: 0.220 g (54 %).

Synthesis of $Y_2(H_2dhtp)(dhtp)(dmf)_2$ (CPO-30): A solid mixture of yttrium nitrate hexahydrate (0.257 g, 0.67 mmol) and 2,5-dihydroxyterephthalic acid (0.133 g, 0.67 mmol) was combined with *N*,*N*-dimethylformamide (12 mL) and water (1 mL) in a Teflon lined stainless steel autoclave and heated to 160 °C for 72 h. The reaction yielded an orange plate-like crystalline substance that was isolated by filtration. Yield: 0.201 g (84 %).

Synthesis of $Y_2(H_2dhtp)(dhtp)(dmf)_2(H_2O)_2\cdot(H_2O)_4$ (CPO-31): A solution of 2,5-dihydroxyterephthalic acid (0.264 g, 1.33 mmol) in *N*,*N*-dimethylformamide (7 mL) is combined with a solution of yttrium nitrate hexahydrate (0.511 g, 1.33 mmol) in water (7 mL) in a Teflon lined stainless steel autoclave and heated to 110 °C for 72 h. The reaction yielded large bright yellow needle-shaped crystals that were isolated by filtration. Yield: 0.236 g (44 %).

Single Crystal X-ray Crystallography: Data of a hemisphere was collected on a Bruker D8 diffractometer with Apex II detector and Oxford Cryosystems Cryostream Plus device. The data was integrated using SAINT and corrected semi-empirically for absorption effects using SADABS.[14] Structure solution was performed using direct methods as implemented in SHELXS.[15] The structures were refined on $|F|^2$ using SHELXL. All non-hydrogen atoms were refined allowing for anisotropic displacement. Hydrogen atoms were assigned to idealized positions and refined with isotropic thermal parameters proportional to the thermal parameter of the atom to which they are attached, except for the hydrogen atoms belonging to the coordinated water molecules and hydroxyl groups which were localized from the difference fourier maps. Their positional and isotropic thermal displacement parameters were freely refined. The hydrogen atoms of the non-coordinated water molecules in CPO-31 were not located. Crystallographic data are summarized in Table 1.

Crystallographic data (excluding structure factors) for the structures in this paper have been deposited with the Cambridge Crystallographic Data Centre, CCDC, 12 Union Road, Cambridge CB21EZ, UK. Copies of the data can be obtained free of charge on quoting the depository numbers CCDC-1999759, CCDC-1999760, and CCDC-1999761. (Fax: +44-1223-336-033; E-Mail: deposit@ccdc.cam.ac.uk, http://www.ccdc.cam.ac.uk)

Variable Temperature Powder X-ray Diffraction: Polycrystalline samples were filled in capillaries of 0.5 mm diameter and measured on a Siemens D5000 diffractometer using monochromatic Cu-Kα_1 radiation (λ = 1.540598 Å). A specially modified sample holder which allows for a flow of gas to pass through the capillary containing the sample was used for the measurements in an atmosphere of nitrogen gas.[16] Measurements in air were performed by using an open capillary. The substance was held in place in the capillary by glass fibers in both cases. The samples were heated by a hot air blower placed underneath the irradiated zone. The temperature was calibrated by measuring silver powder as external or internal standard. Heating rates varied from 5–16 K·h^{-1}. The variable temperature diffraction data was analyzed and processed for presentation with the aid of the program Powder3D.[17]

Supporting Information (see footnote on the first page of this article): Gas adsorption measurements, X-ray powder diffraction of as-synthesized and solvent-exchanged samples, IR spectra.

Results and Discussion

Synthesis

Three different metal-organic frameworks were synthesized from yttrium nitrate and 2,5-dihydroxyterephthalic acid

Table 1. Crystal data and details of structure determination of CPO-29, CPO-30, and CPO-31.

	CPO-29	CPO-30	CPO-31
Formula	$C_{21}H_{27}N_3O_{12}Y$	$C_{11}H_{10}NO_7Y$	$C_{11}H_{12}NO_{10}Y$
M /g·mol^{-1}	602.37	357.11	407.13
T /K	100	100	100
Crystal system	triclinic	monoclinic	monoclinic
Space group	$P\bar{1}$	$P2_1/n$	$P2_1/c$
a /Å	10.4494(8)	13.1316(13)	17.017(2)
b /Å	10.8425(8)	6.5716(7)	9.6608(13)
c /Å	12.5075(9)	15.8017(16)	8.9348(12)
α /°	104.173(1)	90	90
β /°	107.927(1)	98.427(1)	102.774(1)
γ /°	97.527(1)	90	90
V /Å^3	1274.10(16)	1348.9(2)	1432.5(3)
Z	2	4	4
D /g·cm^{-3}	1.570	1.758	1.888
μ /mm^{-1}	2.356	4.353	4.127
2θ range / °	4–54	3.8–55.0	4.8–54.6
No. reflections measured	14190	11056	11822
No. unique reflections	5531	3082	3204
R_{int}	0.042	0.046	0.051
No. observed reflections	4511	2339	2052
No. parameters/restraints	391/0	193/0	217/2
R_1 [$I > 2\sigma(I)$]	0.0376	0.0331	0.0698
wR_2 (all data)	0.0800	0.0815	0.1996
GOF	1.02	1.03	1.07
$\Delta\rho_{min}$ / $\Delta\rho_{max}$ /e Å^{-1}	–0.40/0.59	–0.46/0.61	–1.32/1.81

(H_4dhtp) using mixtures of water and *N*,*N*-dimethylformamide (dmf) as solvent system. Reacting $Y(NO_3)_3{\cdot}6H_2O$, H_4dhtp, water, and dmf in a ratio of 0.67:1:56:155 at 110 °C for 1 d yielded large transparent block shaped colorless to slight yellow crystals which were identified as $Y_2(H_2dhtp)_3(dmf)_4{\cdot}(dmf)_2$ (CPO-29). When the crystals are taken out of the mother liqueur and stored in open atmosphere, they weather and crack quickly, while they hold for extended periods of time in closed containers. Extending the reaction time to three days resulted in the appearance of smaller orange-red crystals on the surface of the large block crystals. This phase was identified as $Y_2(H_2dhtp)(dhtp)(dmf)_2$ (CPO-30). It can be obtained in pure form when the reaction conditions are altered to a ratio of $Y(NO_3)_3{\cdot}6H_2O$:H_4dhtp:H_2O:dmf of 0.67:0.67:56:155, a reaction temperature of 120 or 160 °C and a reaction time of 3 d. We were also able to obtain pure CPO-30 when doubling and tripling the concentration of yttrium nitrate and H_4dhtp and running the reaction at 160 °C for 3 d. When the concentration of water was increased, resulting in a $Y(NO_3)_3{\cdot}6H_2O$:H_4dhtp:H_2O:dmf ratio of 0.67:0.67:389:90, a reaction performed at 110 °C for 3 d yielded large bright yellow crystals of $Y_2(H_2dhtp)(dhtp)(dmf)_2(H_2O)_2{\cdot}(H_2O)_4$ (CPO-31). The yield of this reaction was rather small. It was subsequently enhanced by increasing the concentration of the reactants (resulting in a ratio of the components listed above of 1.33:1.33:389:90). Elevating the temperature to 160 °C yields a spherically grown bright yellow substance which contains an orange crystalline substance in its center.

It is apparent from these observations that the products obtained in the Y^{3+}/H_4dhtp system are highly dependent on the reaction conditions, mainly reactant concentration and ratio, water to dimethylformamide ratio, temperature, and reaction duration. Crystals of CPO-29 form almost immediately when the reaction mixture is prepared and heated. The organic ligand is contained in double deprotonated form in the crystal structure. Consequently, only the carboxylate groups are involved in framework construction, while the hydroxyl groups are available for access from the pores. Upon extended reaction time, CPO-29 starts to transform into the orange compound CPO-30 which contains fewer solvent molecules and equal amounts of completely deprotonated 2,5-dihydroxyterephthalic acid next to the solely bi-deprotonated organic ligand. Higher temperatures further shift the system towards formation of this denser compound, and the compound can be obtained as a pure phase. On the other hand, when the amount of water present in the reaction mixture is increased, another highly condensed phase, CPO-31, forms. It contains additional water as metal coordinated ligand and in the channels. Aside from the solvent content, CPO-30 and CPO-31 are composed of an identical number of metal and organic ligand molecules. Higher temperatures also lead to a partial transformation of CPO-31 into CPO-30, possibly due to removal of water from the structure.

These observations can be summed up in that low temperatures and water concentration and short reaction times lead to the formation of CPO-29, which is the least dense of the three compounds, while a higher water concentration results in formation of the water-rich, more condensed yellow CPO-31. A low water concentration, higher temperature, and longer reaction time yields the more condensed and water-free orange CPO-30. While the actual yttrium to ligand ratio was less important for the observation of these phases, it is preferably adjusted to the ratio in the desired compound to obtain phase pure samples.

Crystal Structure of CPO-29

The framework is constructed from dimeric yttrium coordination polyhedra which are linked through 2,5-dihydroxyterephthalate anions. The two yttrium atoms are linked through four carboxylate groups in a distorted paddle-wheel like arrangement (Figure 1 and animation in the Supporting Information). In half of the paddle-wheel units the C–O–Y angles are similar to the angle found in more regular paddle wheel arrangements and the other half is increased because the metal is displaced sideways due to its larger radius which doesn't allow for closer packing. More regular paddle wheels are found predominantly in copper and zinc compounds in which they are constructed from two square-pyramidal polyhedra whose basal planes face each other.[18] Reflecting the aptitude of yttrium towards higher coordination numbers than zinc and copper, there are four additional ligands (two dimethylformamide molecules and one carboxylate group in pincing mode) instead of the sole apical ligand found in the complexes of the smaller transition metals.

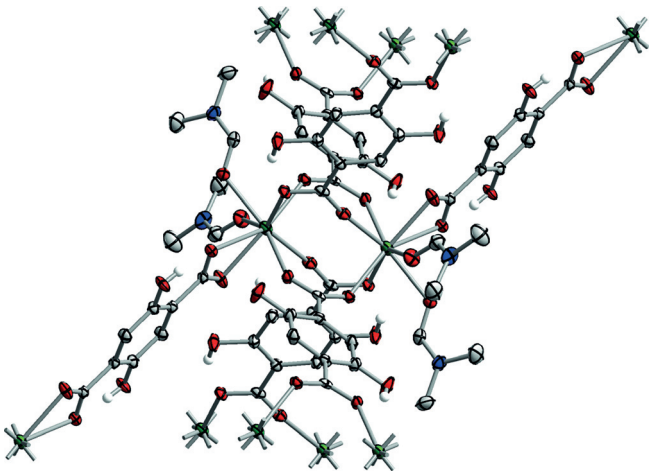

Figure 1. Paddle-wheel like dimeric unit of yttrium coordination polyhedra in CPO-29. Atomic displacement ellipsoids are drawn at the 50 % probability level. Hydrogen atoms are omitted for clarity (except for the hydrogen atoms of the hydroxyl groups). Note the two solvent molecules coordinated to each yttrium atom and the pincing mode carboxylate group.

The dimeric yttrium units are linked in two dimensions by the ligands creating the paddle wheel in bridging mode coordination and in the third by the pincing mode ligand. Thus, a framework with α-polonium topology results (Figure 2 and animation in the Supporting Information). In addition to the two molecules of *N*,*N*-dimethylformamide that are attached to the yttrium atom, there is another crystallographically independent dmf solvent molecule localized in the pore. In total, the solvent molecules occupy 57 % of the volume of the structure.

In Figure 2a, the dimeric yttrium paddle-wheel units are linked horizontally and along the viewing direction by ligands utilizing the carboxylate group in bridging mode coordination, while the ligands with pincing mode coordination of the carboxylate group link the paddle wheel units at a tilted angle within the paper plane. The topology is that of α-polonium.

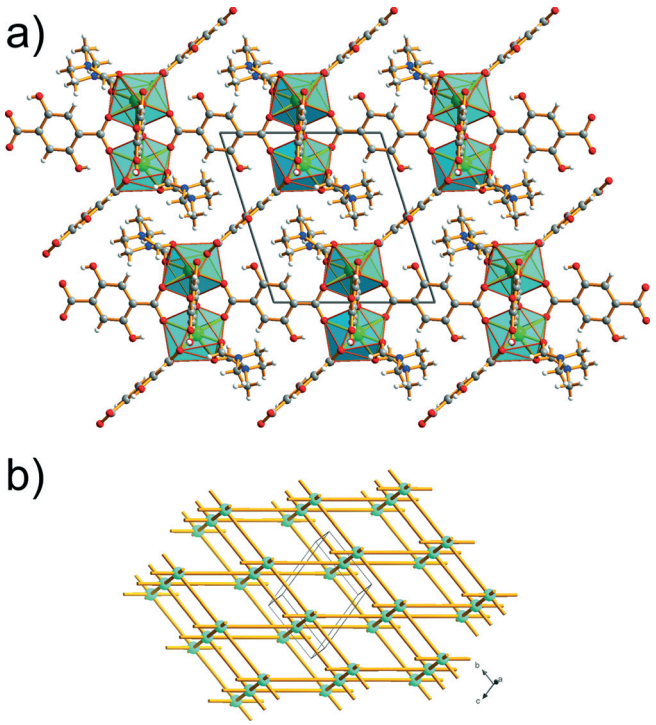

Figure 2. (a) Packing of CPO-29 viewed along [100] (the non-coordinated dmf molecules in the pores are omitted for clarity). (b) Schematic drawing of the pcu-network of CPO-29 (cyan spheres: center of gravity of dimeric yttrium unit, orange cylinders represent the connection between the inorganic SBUs established by the organic linkers).

This network structure has been reported previously for several lanthanide ions[9e–9h,9l,19] and recently also for yttrium.[9i] Because the hydroxy groups do not participate in metal coordination, other ditopic ligands can form compounds with the same network topology; for instance, it has been reported recently for naphthalene-2,6-dicarboxylate.[20]

Crystal Structure of CPO-30

The organic linker is incorporated in two different states of deprotonation in the orange compound CPO-30. One of the linking molecules is fully deprotonated, e.g. all four hydroxyl and carboxylic acid groups are transformed into the respective conjugated base group, and all of these are involved in coordination of the yttrium ion. The second organic molecule contains only the carboxylate groups as anionic functional group, while the hydroxyl groups remain protic and are not involved in framework construction. Instead, it is engaged in an intramolecular hydrogen bond to the closest carboxylate oxygen atom. The organic linkers connect the yttrium atoms into a three-dimensional network which contains undulating chains of condensed yttrium polyhedra and parallel one-dimensional channels (Figure 3a). The yttrium atom is again eight-coordinate, with seven coordinated oxygen atoms originating from the organic linker and the eighth from a coordinated *N*,*N*-dimethylformamide molecule, which reaches into the channel. In fact, the channels are completely occupied by these coordinated solvent molecules. They are bonded in alternating fash-

ion to yttrium atoms in opposing corners of the rhombic channel. The channel volume accounts for 43 % of the total volume. In the projection along the channels, it becomes apparent that the framework is constructed by chains of condensed yttrium coordination polehydra at the corners of the parallelepiped surrounding the solvent area, and the organic linker composes the edges of the parallelepiped. The H_2dhtp^{2-} and the $dhtp^{4-}$ ligands are arranged in lamellar fashion along the faces of the channel walls. They are ordered in a fashion that all the H_2dhtp^{2-} ligands are arranged along two of the four faces of the channel and all the $dhtp^{4-}$ ligands are arranged along the other two faces. The two walls with the ligand in the same state of deprotonation are in *trans* position to each other when viewed with the chains of metal coordination polyhedra as center (Figure 3b).

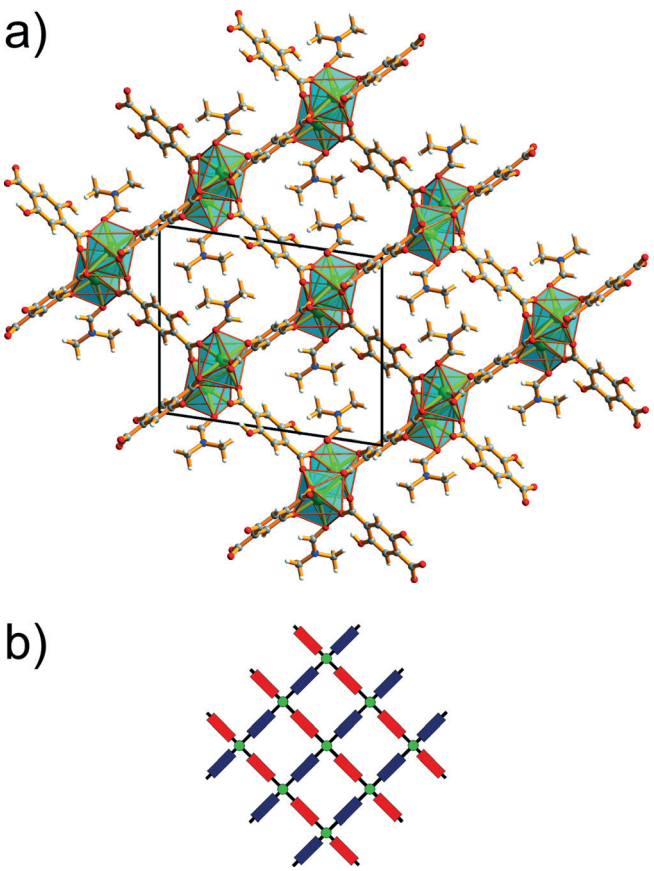

Figure 3. (a) View of CPO-30 along [010] showing the one-dimensional channels which are filled with dmf solvent molecules coordinated to the yttrium atom. (b) Schematic representation of the connectivity in CPO-30 (green circles: inorganic SBU, red bars: 2,5-dihydroxyterephthalate, blue bars: 2,5-dioxidoterephthalate).

The functional groups of the organic ligand exhibit a number of coordination modes in their bonding to the metal (Figure 4 and animation in the Supporting Information). The carboxylate group of the fully deprotonated linker coordinates an yttrium atom in pincing mode, thus accounting for two of the coordination bonds. Each of the oxygen atoms of this carboxylate group is coordinated to an adjacent yttrium atom in the chain by a sideways bond, accounting for another two bonding partners of the yttrium (as there are two such molecules on opposite sides of the chain of metal coordination polyhedrae). Another bond stems from the oxygen atom of the deprotonated hydroxyl group. This forms a six-ring chelate together with one of the sideways carboxylate-O coordination bonds. The metal coordination is completed by two bonds with carboxylate oxygen atoms from the partly deprotonated organic linker. These carboxylate groups coordinate two yttrium atoms in bridging mode, like in the paddle-wheel motif of CPO-29, with one bridge extending to each of the two neighboring yttrium atoms in the chain. The eightfold yttrium coordination polyhedra are condensed to undulating chains through common edges which are made up by the oxygen atoms of the pincing mode carboxylate group. CPO-30 is isostructural to the terbium-organic framework SION-1.[9h]

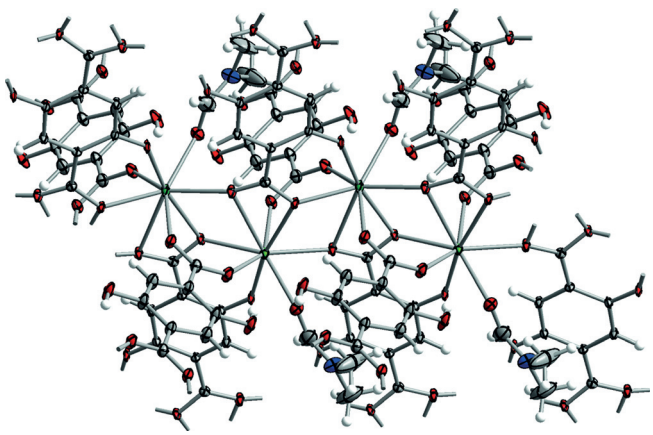

Figure 4. View of CPO-30 along the chain showing the coordination modes of the organic ligand and the environment of the yttrium (atomic displacement ellipsoids drawn at 70 % probability for Y and at 50 % probability for the remaining non-hydrogen atoms).

Crystal Structure of CPO-31

Like CPO-30, this compound contains two different organic linking molecules, in which either both hydroxyl and carboxylic acid groups have become deprotonated or it contains protonated hydroxyl groups and carboxylate groups. Furthermore, CPO-31 also contains one-dimensional channels within the three-dimensional framework constructed of the organic linkers and yttrium polyhedra which also are condensed to chains along the corners of the parallelepiped which forms the circumference of the channels (Figure 5a). The yttrium atom is again eight-coordinate. However, and in contrast to CPO-30, only six of the oxygen atoms coordinated to the metal are part of an organic linker. The remaining two belong to one water molecule and one dmf molecule, respectively, which point into the channel. In addition, there are non-coordinated water molecules occupying part of the channel. It is intriguing to note that the solvent area is divided up into a region occupied by the more hydrophobic part of the organic solvent and one occupied by water. As in CPO-30, the volume of the solvent area accounts for 43 % of the unit cell volume.

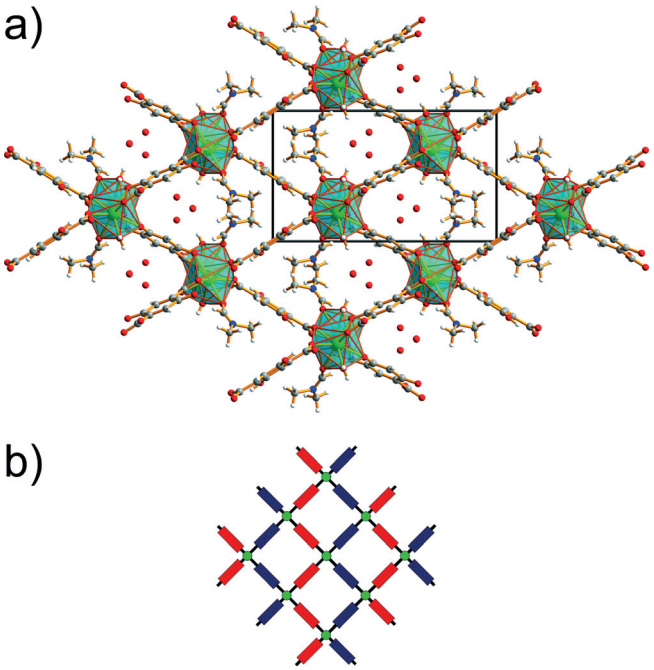

Figure 5. (a) View of CPO-31 along [001]. Note the distinct solvent areas of water and dmf within the channels. (b) Schematic representation of the connectivity in CPO-30 (green circles: inorganic SBU, red bars: 2,5-dihydroxyterephthalate, blue bars: 2,5-dioxidoterephthalate).

Like in CPO-30, only organic linker of the same deprotonation state is found along the individual walls of the channel. However, the two walls with H_2dhtp^{2-} and $dhtp^{4-}$ ligand, respectively, are in *cis*-position to each other in CPO-31, rather than in *trans*-position as in CPO-30 (Figure 5b). The close structural relationship between CPO-30 and CPO-31 is also reflected in the larger degree of similarity of their IR spectra in comparison to that of CPO-29 (Figure S8, Supporting Information).

Both compounds have the composition $Y_2(H_2dhtp)(dhtp)$ upon hypothetical removal of the coordinated and non-coordinated (if present) solvent. Thus, the frameworks of CPO-30 and CPO-31 are an example for polymorphism in metal-organic frameworks.[21]

The additional coordinated solvent molecule results in a different utilization of coordination modes of the organic linker in CPO-31 than in CPO-30 because of the reduced number of bonding interactions needed to complete the coordination sphere around the yttrium atom (Figure 6 and animations in the Supporting Information). The carboxylate group of the H_2dhtp^{2-} ligand coordinates two yttrium atoms in bridging mode similar to the paddle wheel unit in CPO-29. Because there are two of these ligands in *cis*-position to each other, this type of bonding interaction accounts for two of the six bonds at each yttrium atom donated from the organic linker. The remaining four bonds are donated from the fully deprotonated $dhtp^{4-}$ ligand, two from the carboxylate group coordinating an yttrium atom in pincing mode and another two from a chelating coordination through the α-oxocarboxylate group. The carboxylate-yttrium interaction of this six-ring is again a sideways donation from the carboxylate group which is pincing the adjacent yttrium atom. A second sideways coordination bond of this carboxylate group that is present in CPO-30 is absent in CPO-31.

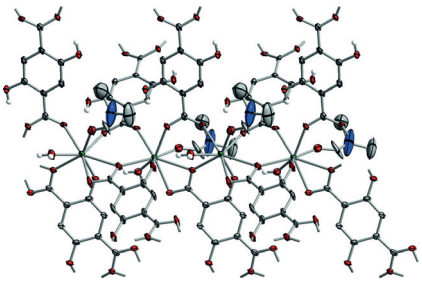

Figure 6. View of CPO-31 along the chain showing the coordination modes of the organic ligand and the environment of the yttrium (atomic displacement ellipsoids drawn at 70% probability for Y and at 50% probability for the remaining non-hydrogen atoms).

Thermogravimetry

CPO-29

The weight of CPO-29 stays initially constant upon heating (Figure 7a, blue trace). A noticeably decrease in weight sets in only above 90 °C. (However, the observation of relatively quick weathering of crystals stored openly in ambient atmosphere indicates that solvent is easily evaporated from CPO-29.) The TG trace then contains three distinct steps ending at 144, 209, and 261 °C, respectively. They correspond exactly with the three dmf solvent molecules contained in the structure. However, there are no developed plateaus to be observable in between the individual steps. Thus, solvent removal by and large occurs continuously for this material. The distinction between the steps also diminishes progressively. The end of the third step is almost non-observable, because the weight loss continues at a similar rate, now indicative of decomposition of the remaining framework. The powder pattern taken after the TG run shows the presence of nanometer sized yttrium oxide Y_2O_3.

A sample of CPO-29 was placed in methanol to replace the high-boiling dmf with solvent which can be removed under milder conditions in an attempt to activate the material for gas adsorption. In fact, the corresponding TG trace (Figure 7a, green line) indicates immediate and rapid removal of solvent. It is already complete at 80 °C, slightly above the boiling point of methanol. The subsequent plateau extends till approximately 210 °C, above which the framework starts to disintegrate. The methanol exchanged material has a significantly changed powder X-ray diffraction pattern (Figure S4, Supporting Information).

CPO-30

The TG trace of the as-prepared CPO-30 material (Figure 7b, blue line) shows even less change in the beginning of the experiment than CPO-29. Except for a small initial weight loss possibly due to solvent attached on the outer surface of

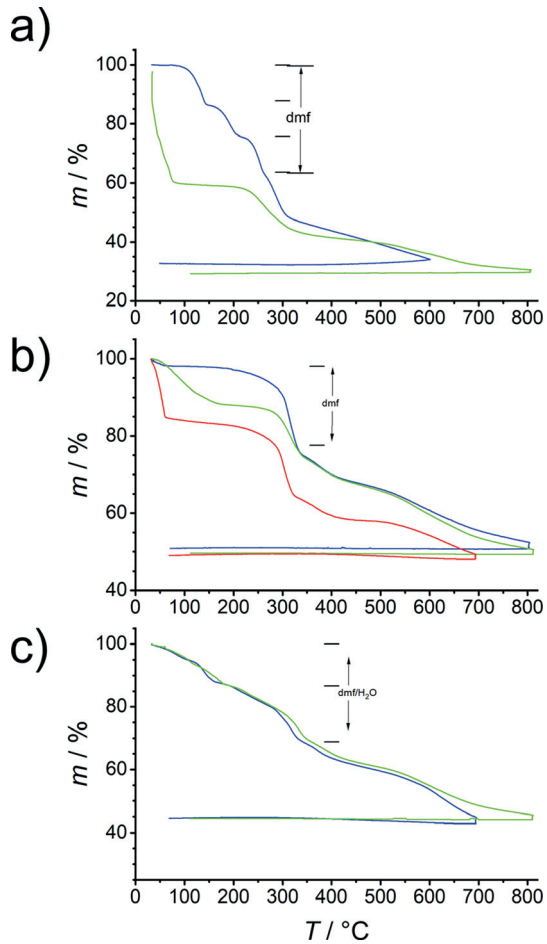

Figure 7. TG traces of (a) CPO-29; (b) CPO-30; and (c) CPO-31 in nitrogen atmosphere (blue: as-prepared, red/green: methanol exchanged samples).

the substance, the weight stays unchanged until approximately 180 °C, which is above the boiling point of dmf. This attests to how strongly bound the coordinated dmf molecule is within the structure. Above 180 °C, an increasing rate of weight loss is observed until weight corresponding to the amount of solvent has been removed at ~330 °C. Subsequently, the weight decreases at a slower rate during decomposition of the material to Y_2O_3 as identified by powder X-ray diffraction.

The CPO-30 material has also been immersed in methanol with the purpose of exchanging the coordinated solvent molecules. The treated samples again show weight loss at lower temperatures than the as-prepared material. In one case (Figure 7b, green trace) it appears that the treatment has not resulted in complete exchange of the solvent because the weight loss occurs much less rapidly than in the second case (Figure 7b, red trace) in which it is similarly quick as in the case of CPO-29. It gives way to a plateau-like range until decomposition of the remaining framework occurs. Surprisingly, the sample which was obviously solvent exchanged to a higher degree had been immersed for a shorter duration (6 d vs. 9 d, respectively). Because both samples originated in different batches of the CPO-30 material this may be due to crystallite size effects which are expected to have a major impact on the diffusivity within the one-dimensional channels, especially considering the strong interaction between framework and solvent since all of the solvent molecules are coordinated to yttrium atoms. (However, the possibility of a structural transformation as discussed below will also account for this behavior.)

CPO-31

In contrast to the other two compounds, CPO-31 exhibits weight loss immediately when the measurement begins (Figure 7c, blue trace). This is probably due to the presence of the water in the channels of the structure. The water can be more easily removed than the higher boiling dmf. An inflection point is observed at ca. 160 °C when the weight loss is corresponding to the three water molecules present in the compound. The weight continues to decrease without interruption with the loss of the dmf molecule, which is complete at 342 °C by weight and presence of another inflection point. However, this is again immediately followed by a further reduction in weight indicating decomposition of the compound to yttrium oxide. A sample which was immersed in methanol has a similar TG trace (Figure 7c, green trace) indicating that the attempt to exchange the pore content was not successful.

Variable Temperature Powder X-ray Diffraction

CPO-29

The powder X-ray diffraction pattern of CPO-29 (Figure 8) shows a number of changes upon heating in a stream of inert gas. The structure crystallizes in the triclinic crystal system. Thus, it can easily accommodate changes in the solvent content of the structure by adjusting any of the lattice parameters. When heating commences, the first four reflection quickly reveal a fifth, when the coincidental superposition of the (1 0 $\bar{1}$) and (0 1 $\bar{1}$) reflection is removed. At ~100 °C, a second phase appears in the powder pattern which subsequently transforms into a third phase. This process is completed at 170 °C,

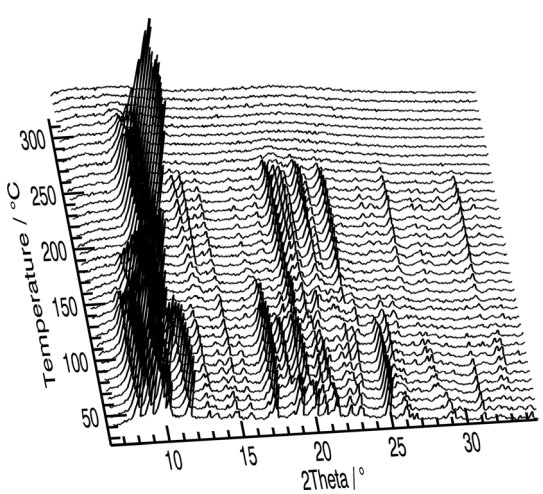

Figure 8. Variable temperature powder X-ray diffraction patterns of CPO-29 measured in a stream of nitrogen gas and a heating rate of 16 K·h^{-1}.

slightly above the boiling point of dmf. The powder pattern of this phase looks simpler than that of the triclinic parent compound, indicating that the emptier structure might crystallize with higher symmetry. Unfortunately, the data quality of this experiment didn't permit a full structure determination. The third phase remains basically unchanged until 219 °C. Subsequently, the maximum intensity of the strongest reflection diminishes rapidly until no crystalline material is observed anymore at ~300 °C.

A comparison of the occurrences of the phase transitions with the distinct steps observed in the TG curve of CPO-29 shows that they roughly correspond under the assumption that the temperatures in the diffraction experiment are shifted toward lower temperatures because of the slower heating rate in respect to the TG experiment. The first phase which is exclusively present below 100 °C in the powder patterns reflects the initial structure while it loses the non-coordinated solvent molecule. The second phase then corresponds to a structure which has accommodated the initial solvent loss and exists during the removal of the first of the two coordinated dmf molecules. The third phase which was exclusively present and stable in the temperature range of 170 to 219 °C then is representative of the material with one dmf molecule remaining at the yttrium atom. Above this temperature, when the final solvent molecule has become abscised from the metal atom, the crystallinity of the material is lost quickly, as already indicated by the continuous transition from solvent removal to framework decomposition in the TG curve at 261 °C.

CPO-30

The powder X-ray diffraction pattern of CPO-30 (Figure 9) stays virtually constant upon increasing temperature which is in accordance to the negligible weight loss observed for the as-synthesized compound below 200 °C. The structure consequently changes very little during this process, which we confirmed by a single crystal structure determination performed at 180 °C. It indicated the coordinated solvent molecules at the yttrium are still present at this temperature. Subsequently, the intensities of the reflections start to decrease at ~200 °C until the crystallinity has been completely lost.

In contrast, the long range order of the material disappears already at 80 °C in air. Such a diminished stability in air is typical for 2,5-dihydroxyterephthalic acid based metal-organic frameworks with open metal sites. Because the cation is not amenable to undergo redox reactions easily, we ascribe it to an oxidative attack of oxygen from air on the organic linker which, after all, carries a hydroquinone functionality commonly known to be susceptible to being oxidized to a quinoid system.

CPO-31

In the case of CPO-31 (Figure 10), an overall drop in intensity occurs already between 40 and 53 °C, while the phase apparently stays the same. A second phase is first observed at 70 °C. It has replaced the first phase completely at ca. 120 °C.

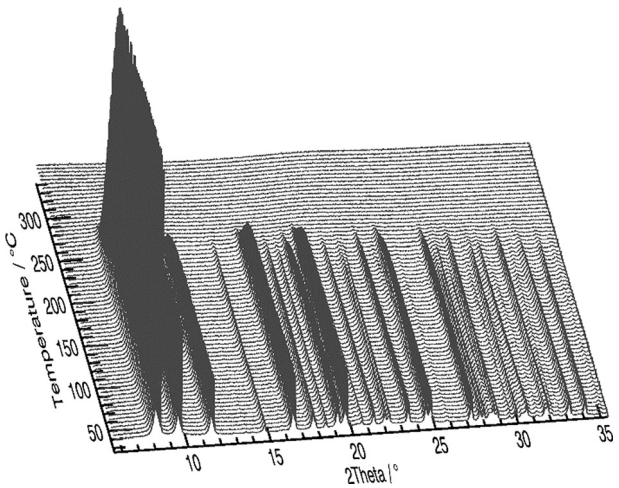

Figure 9. Variable temperature powder X-ray diffraction patterns of CPO-30 measured in a stream of nitrogen gas and a heating rate of 5 K·h^{-1}.

Its reflections become more pronounced afterwards, but overall they are significantly less intense than those of the first phase. Starting from 215 °C, the reflection intensities decrease, though there still is a remnant of the most intense one at 340 °C, when the experiment was terminated.

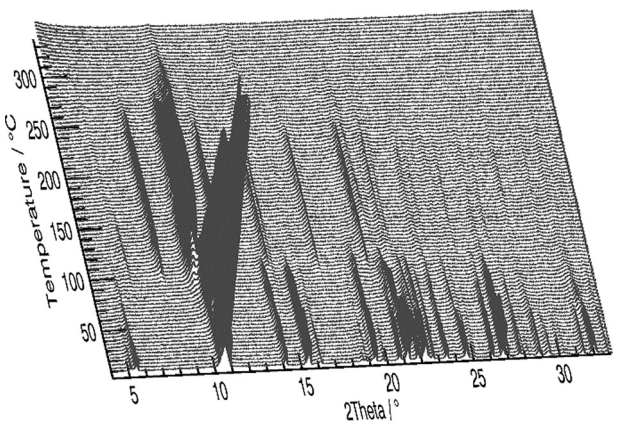

Figure 10. Variable temperature powder X-ray diffraction patterns of CPO-31 measured in a stream of nitrogen gas and a heating rate of 8 K·h^{-1}.

The phase transition is in all likelihood due to the loss of the water molecules in the channels and on the yttrium atom, which was complete at ~160 °C in the TG experiment with higher heating rate. The water free compound obviously has a different structure which remains stable until above 200 °C, possibly as long as the dmf molecule is bound to the yttrium atom. Afterwards, the crystallinity is lost immediately as exemplified by the absence of a plateau after solvent removal in the TG curve.

Gas Adsorption

All three metal-organic frameworks presented here have solvent filled volume. Consequently, attempts were made to acti-

vate the material and access the internal volume by nitrogen gas adsorption. However, these attempts were unsuccessful except for CPO-30.

CPO-29

Because the TG curve of CPO-29 indicates a seamless progression from removal of the *N*,*N*-dimethylformamide to decomposition of the framework, the solvent was exchanged with methanol prior to the gas adsorption experiment. The powder diffraction pattern of the solvent exchanged sample (Figure S4, Supporting Information) is still well crystalline. The reflection positions have shifted distinctly as a result of the accommodation of the flexible framework towards solvent replacement. The subsequent gas adsorption experiment yielded no discernible microporous surface area (Figure S1a, Supporting Information). The powder pattern of the material after activation and adsorption experiment reveals a significant shift of the first reflections towards smaller d spacing (Figure S4, Supporting Information). This might indicate a contraction of the framework upon solvent removal, which can make the pore inaccessible towards the nitrogen molecule. Such phenomena are well known from breathing compounds like MIL-53.[22]

CPO-31

Like the TG curves, the powder X-ray diffraction patterns of the as-synthesized and the methanol exchanged CPO-31 material are nearly identical (Figure S6, Supporting Information). This already indicates that the solvent exchange was probably unsuccessful. Accordingly, no microporosity was detected for the material (Figure S1c, Supporting Information). The thermodiffraction shows that a discontinuous phase transition occurs on heating, probably meaning the crystal structure responds flexibly to removal of the solvent. While the actual crystal structure of the high temperature phase could not be determined, it may well be that it doesn't allow access to the pore in the adsorption experiment.

CPO-30

The as-synthesized CPO-30 material also does not show any gas uptake confirming porosity (Figure S1b, Supporting Information). This is not surprising, considering that the single crystal structure of the sample measured at 180 °C still contained most of the solvent. In contrast, a BET and Langmuir specific surface area of 272 and 324 $m^2 \cdot g^{-1}$, respectively, and pore volume of 0.11 $cm^3 \cdot g^{-1}$ were determined for the sample which was methanol exchanged for 6 days and activated at 120 °C in a dynamic vacuum. An estimation of the pore volume using the unit cell volume of the as-synthesized material and the solvent area yields 0.31 $cm^3 \cdot g^{-1}$. The powder X-ray diffraction pattern of the methanol-exchanged material does indicate a degree of flexibility in the structural upon solvent exchange (Figure S5, Supporting Information), but the peak shifts are not sufficient to account for such a large difference in pore volume. Thus, it appears that not all of the microporous volume was accessible to the probe molecule, e.g. the dmf was not completely replaced by methanol during the solvent exchange, as can also be deduced from the TG curve of the methanol exchanged sample. The presence of a few dimethylformamide molecules suffices in blocking an entire channel, and complete activation is therefore crucial to access the full pore volume of the material.

However, higher activation temperatures increase the danger of inducing the collapse of the framework. Indeed, a lower BET and Langmuir specific surface area of 161 and 196 $m^2 \cdot g^{-1}$, respectively, and pore volume of 0.07 $cm^3 \cdot g^{-1}$ was obtained when the activation temperature was increased to 200 °C for the same sample. The powder pattern of this material looks somewhat less crystalline, too (Figure S5, Supporting Information). It would be possible to employ milder activation procedures if the solvent in the pores was completely replaced by methanol. However, extending the duration of immersion in methanol to 9 days resulted in a material which showed no microporosity after mild activation at room temperature in a dynamic vacuum for 1600 min. As discussed on the basis of the TG curves, this could be due to less complete solvent exchange than for the sample exposed to methanol for 6 days because the two samples came from different batches. Differences in crystallite size and the dependency of the diffusion on it may well have such an effect. However, the powder pattern of the material treated for 9 days with methanol shows reflections congruent with CPO-31 in addition to those of CPO-30 and further unidentified reflections (Figure S7, Supporting Information). It seems as if prolonged exposure leads to a partial transformation of the framework structure. This is facile enough as the two frameworks are structurally similar, as discussed above. Since CPO-31 does not show any gas uptake related to microporosity, and transformation of the structure would begin at the pore openings, this can explain the non-accessibility of the pore volume in the adsorption experiment. The sample was subsequently activated at 105 °C in a dynamic vacuum for 900 min., but still showed no microporosity. Intriguingly, though, the reflections concomitant with CPO-31 diminished in intensity, indicating that the structural transformation is reversible.

On the basis of these observations, CPO-30 appears to be the most promising of the three materials in respect to achieving accessibility to the internal pore volume. Coincidentally, it is the only one of the three compounds not showing a phase transition in the variable temperature powder X-ray diffraction experiment. This rigidity of the framework might be related to the fact that the yttrium atoms in CPO-30 carry only one coordinated solvent molecule, while the departure of two solvent molecules per yttrium atom in CPO-29 and CPO-31 naturally impart a greater propensity towards rearranging the coordination environment of the metal atom and consequently of the structure. However, a correct activation procedure needs to fully replace the dmf in the pores with a more easily removable solvent, while avoiding induction of structural transformations.

Conclusions

We have presented three metal-organic frameworks based on yttrium and 2,5-dihydroxyterephthalic acid. Which material

forms is dependent on the reaction conditions, further illustrating the immense structural diversity that exists for metal-organic framework compounds with yttrium(III) and related lanthanide ions and a multidentate ligand like 2,5-dihydroxyterephthalic acid.[9d–9i,9l] All three crystal structures contain large volumes filled with solvent, though we only managed to demonstrate a limited degree of permanence of porosity for CPO-30. The desolvated framework structures of CPO-30 and CPO-31 are polymorphic; the as-synthesized compounds differ in solvent content. The compounds show widely differing behavior upon heat treatment, as evidenced by the occurrence of phase transitions during desolvation, and the flexibility of the framework structure indicated by these might be the reason for inaccessibility of the pores. Yttrium and lanthanide compounds are frequently isostructural. Doped yttrium (or, in fact, pure) lanthanide MOFs with 2,5-dihydroxyterepthalic acid as organic component can show a wide variation within their optical and magnetic properties, which can be exploited in sensing and imaging applications.[9m,23] Thus, the materials reported here are a valuable expansion of the library of available compounds for research in these directions.

Acknowledgements

We thank *Egil Nodland* for recording the IR spectra and the Research Council of Norway for support (NANOMAT project 182056/S10).

Keywords: Metal-organic frameworks; Yttrium; 2,5-Dihydroxyterephthalic acid; Microporous materials; X-ray diffraction; Polymorphism

References

[1] a) R.-B. Lin, S. Xiang, H. Xing, W. Zhou, B. Chen, *Coord. Chem. Rev.* **2019**, *378*, 87–103; b) M. Ding, R. W. Flaig, H.-L. Jiang, O. M. Yaghi, *Chem. Soc. Rev.* **2019**, *48*, 2783–2828; c) H. Li, K. Wang, Y. Sun, C. T. Lollar, J. Li, H.-C. Zhou, *Mater. Today* **2018**, *21*, 108–121; d) M. J. Kalmutzki, C. S. Diercks, O. M. Yaghi, *Adv. Mater.* **2018**, *30*, 1704304; e) L. E. Kreno, K. Leong, O. K. Farha, M. Allendorf, R. P. Van Duyne, J. T. Hupp, *Chem. Rev.* **2012**, *112*, 1105–1125; f) F.-Y. Yi, D. Chen, M.-K. Wu, L. Han, H.-L. Jiang, *ChemPlusChem.* **2016**, *81*, 675–690; g) W. P. Lustig, S. Mukherjee, N. D. Rudd, A. V. Desai, J. Li, S. K. Ghosh, *Chem. Soc. Rev.* **2017**, *46*, 3242–3285; h) I. Stassen, N. Burtch, A. Talin, P. Falcaro, M. Allendorf, R. Ameloot, *Chem. Soc. Rev.* **2017**, *46*, 3185–3241; i) Q. Wang, D. Astruc, *Chem. Rev.* **2020**, *120*, 1438–1511; j) S. M. J. Rogge, A. Bavykina, J. Hajek, H. Garcia, A. I. Olivos-Suarez, A. Sepulveda-Escribano, A. Vimont, G. Clet, P. Bazin, F. Kapteijn, M. Daturi, E. V. Ramos-Fernandez, F. X. Llabres i Xamena, V. Van Speybroeck, J. Gascon, *Chem. Soc. Rev.* **2017**, *46*, 3134–3184; k) Y. He, F. Chen, B. Li, G. Qian, W. Zhou, B. Chen, *Coord. Chem. Rev.* **2018**, *373*, 167–198; l) Y. He, W. Zhou, G. Qian, B. Chen, *Chem. Soc. Rev.* **2014**, *43*, 5657–5678.

[2] a) R. E. Morris, L. Brammer, *Chem. Soc. Rev.* **2017**, *46*, 5444–5462; b) M. O'Keeffe, O. M. Yaghi, *Chem. Rev.* **2012**, *112*, 675–702; c) D. Zhao, D. J. Timmons, D. Yuan, H.-C. Zhou, *Acc. Chem. Res.* **2011**, *44*, 123–133.

[3] a) Y. Yan, C. Li, Y. Wu, J. Gao, Q. Zhang, *J. Mater. Chem. A* **2020**, *8*, 15245–15270; b) Z. Chen, S. L. Hanna, L. R. Redfern, D. Alezi, T. Islamoglu, O. K. Farha, *Coord. Chem. Rev.* **2019**, *386*, 32–49; c) S. Yuan, J.-S. Qin, C. T. Lollar, H.-C. Zhou, *ACS Cent. Sci.* **2018**, *4*, 440–450; d) H. Assi, G. Mouchaham, N. Steunou, T. Devic, C. Serre, *Chem. Soc. Rev.* **2017**, *46*, 3431–3452; e) C. Healy, K. M. Patil, B. H. Wilson, L. Hermanspahn, N. C. Harvey-Reid, B. I. Howard, C. Kleinjan, J. Kolien, F. Payet, S. G. Telfer, P. E. Kruger, T. D. Bennett, *Coord. Chem. Rev.* **2020**, *419*, 213388; f) S. L. Griffin, N. R. Champness, *Coord. Chem. Rev.* **2020**, *414*, 213295.

[4] N. E. Ghermani, G. Morgant, J. d'Angelo, D. Desmaele, B. Fraisse, F. Bonhomme, E. Dichi, M. Sgahier, *Polyhedron* **2007**, *26*, 2880–2884.

[5] C. D. Ene, F. Tuna, O. Fabelo, C. Ruiz-Pérez, A. M. Madalan, H. W. Roesky, M. Andruh, *Polyhedron* **2008**, *27*, 574–582.

[6] P. D. C. Dietzel, R. Blom, H. Fjellvåg, *Eur. J. Inorg. Chem.* **2008**, 3624–3632.

[7] P. D. C. Dietzel, R. Blom, H. Fjellvåg, *Dalton Trans.* **2006**, 2055–2057.

[8] a) C. Serre, F. Millange, S. Surblé, G. Férey, *Angew. Chem. Int. Ed.* **2004**, *43*, 6285–6289; b) A. C. Sudik, A. P. Côté, O. M. Yaghi, *Inorg. Chem.* **2005**, *44*, 2998–3000; c) C. Serre, C. Mellot-Draznieks, S. Surblé, N. Audebrand, Y. Filinchuk, G. Férey, *Science* **2007**, *315*, 1828–1831.

[9] a) P. D. C. Dietzel, R. Blom, H. Fjellvåg, *Z. Anorg. Allg. Chem.* **2009**, *635*, 1953–1958; b) P.-C. Liang, H.-K. Liu, C.-T. Yeh, C.-H. Lin, V. Zima, *Cryst. Growth Des.* **2011**, *11*, 699–708; c) A. Douvali, G. S. Papaefstathiou, M. P. Gullo, A. Barbieri, A. C. Tsipis, C. D. Malliakas, M. G. Kanatzidis, I. Papadas, G. S. Armatas, A. G. Hatzidimitriou, T. Lazarides, M. J. Manos, *Inorg. Chem.* **2015**, *54*, 5813–5826; d) K. L. Gurunatha, S. Mohapatra, P. A. Suchetan, T. K. Maji, *Cryst. Growth Des.* **2009**, *9*, 3844–3847; e) S. Nayak, H. P. Nayek, C. Pietzonka, G. Novitchi, S. Dehnen, *J. Mol. Struct.* **2011**, *1004*, 82–87; f) Y.-L. Wang, Y.-L. Jiang, Q.-Y. Liu, Y.-X. Tan, J.-J. Wei, J. Zhang, *CrystEngComm* **2011**, *13*, 4981–4987; g) Y.-L. Wang, Y.-L. Jiang, Z.-J. Xiahou, J.-H. Fu, Q.-Y. Liu, *Dalton Trans.* **2012**, *41*, 11428–11437; h) S. L. Anderson, A. Gladysiak, P. G. Boyd, C. P. Ireland, P. Mieville, D. Tiana, B. Vlaisavljevich, P. Schouwink, W. van Beek, K. J. Gagnon, B. Smit, K. C. Stylianou, *CrystEngComm* **2017**, *19*, 3407–3413; i) J. De Bellis, D. Belli Dell'Amico, G. Ciancaleoni, L. Labella, F. Marchetti, S. Samaritani, *Inorg. Chim. Acta* **2019**, *495*, 118937; j) K. Jayaramulu, P. Kanoo, S. J. George, T. K. Maji, *Chem. Commun.* **2010**, *46*, 7906–7908; k) Q.-G. Zhai, X. Bu, C. Mao, X. Zhao, L. Daemen, Y. Cheng, A. J. Ramirez-Cuesta, P. Feng, *Nat. Commun.* **2016**, *7*, 13645; l) J. De Bellis, L. Bellucci, G. Bottaro, L. Labella, F. Marchetti, S. Samaritani, D. Belli Dell'Amico, L. Armelao, *Dalton Trans.* **2020**, *49*, 6030–6042; m) D. F. Sava Gallis, L. E. S. Rohwer, M. A. Rodriguez, M. C. Barnhart-Dailey, K. S. Butler, T. S. Luk, J. A. Timlin, K. W. Chapman, *ACS Appl. Mater. Interfaces* **2017**, *9*, 22268–22277.

[10] a) P. D. C. Dietzel, R. E. Johnsen, R. Blom, H. Fjellvåg, *Chem. Eur. J.* **2008**, *14*, 2389–2397; b) P. D. C. Dietzel, Y. Morita, R. Blom, H. Fjellvåg, *Angew. Chem. Int. Ed.* **2005**, *44*, 6354–6358; c) P. D. C. Dietzel, B. Panella, M. Hirscher, R. Blom, H. Fjellvåg, *Chem. Commun.* **2006**, 959–961; d) N. L. Rosi, J. Kim, M. Eddaoudi, B. Chen, M. O'Keeffe, O. M. Yaghi, *J. Am. Chem. Soc.* **2005**, *127*, 1504–1518; e) W. Zhou, H. Wu, T. Yildirim, *J. Am. Chem. Soc.* **2008**, *130*, 15268–15269; f) E. D. Bloch, L. J. Murray, W. L. Queen, S. Chavan, S. N. Maximoff, J. P. Bigi, R. Krishna, V. K. Peterson, F. Grandjean, G. J. Long, B. Smit, S. Bordiga, C. M. Brown, J. R. Long, *J. Am. Chem. Soc.* **2011**, *133*, 14814–14822; g) M. Märcz, R. E. Johnsen, P. D. C. Dietzel, H. Fjellvåg, *Microporous Mesoporous Mater.* **2012**, *157*, 62–74; h) R. Sanz, F. Martinez, G. Orcajo, L. Wojtas, D. Briones, *Dalton Trans.* **2013**, *42*, 2392–2398.

[11] a) J. G. Vitillo, L. Regli, S. Chavan, G. Ricchiardi, G. Spoto, P. D. C. Dietzel, S. Bordiga, A. Zecchina, *J. Am. Chem. Soc.* **2008**, *130*, 8386–8396; b) Y. Liu, H. Kabbour, C. M. Brown, D. A. Neumann, C. C. Ahn, *Langmuir* **2008**, *24*, 4772–4777; c) A. G. Wong-Foy, A. J. Matzger, O. M. Yaghi, *J. Am. Chem. Soc.* **2006**, *128*, 3494–3495; d) P. D. C. Dietzel, P. A. Georgiev, J. Eck-

ert, R. Blom, T. Strässle, T. Unruh, *Chem. Commun.* **2010**, *46*, 4962–4964; e) S. A. FitzGerald, B. Burkholder, M. Friedman, J. B. Hopkins, C. J. Pierce, J. M. Schloss, B. Thompson, J. L. C. Rowsell, *J. Am. Chem. Soc.* **2011**, *133*, 20310–20318; f) M. H. Rosnes, M. Opitz, M. Frontzek, W. Lohstroh, J. P. Embs, P. A. Georgiev, P. D. C. Dietzel, *J. Mater. Chem. A* **2015**, *3*, 4827–4839; g) J. Y. Kim, R. Balderas-Xicohténcatl, L. Zhang, S. G. Kang, M. Hirscher, H. Oh, H. R. Moon, *J. Am. Chem. Soc.* **2017**, *139*, 15135–15141.

[12] a) S. R. Caskey, A. G. Wong-Foy, A. J. Matzger, *J. Am. Chem. Soc.* **2008**, *130*, 10870–10871; b) P. D. C. Dietzel, R. E. Johnsen, H. Fjellvåg, S. Bordiga, E. Groppo, S. Chavan, R. Blom, *Chem. Commun.* **2008**, 5125–5127; c) D. Yu, A. O. Yazaydin, J. R. Lane, P. D. C. Dietzel, R. Q. Snurr, *Chem. Sci.* **2013**, *4*, 3544–3556; d) W. L. Queen, M. R. Hudson, E. D. Bloch, J. A. Mason, M. I. Gonzalez, J. S. Lee, D. Gygi, J. D. Howe, K. Lee, T. A. Darwish, M. James, V. K. Peterson, S. J. Teat, B. Smit, J. B. Neaton, J. R. Long, C. M. Brown, *Chem. Sci.* **2014**, *5*, 4569–4581; e) B. Pato-Doldán, M. H. Rosnes, P. D. C. Dietzel, *ChemSusChem* **2017**, *10*, 1710–1719.

[13] a) F. Lundvall, P. Vajeeston, D. S. Wragg, P. D. C. Dietzel, H. Fjellvåg, *Cryst. Growth Des.* **2016**, *16*, 339–346; b) F. Lundvall, D. S. Wragg, P. Vajeeston, P. D. C. Dietzel, H. Fjellvag, *CrystEngComm* **2017**, *19*, 5857–5863; c) A. A. Bezrukov, K. W. Törnroos, P. D. C. Dietzel, *Eur. J. Inorg. Chem.* **2016**, *2016*, 4430–4439.

[14] a) Bruker AXS: Madison, WI, **2004**; b) Bruker AXS: Madison, WI, **2004**.

[15] G. M. Sheldrick, University of Göttingen, Germany, **1997**.

[16] P. Norby, *J. Am. Chem. Soc.* **1997**, *119*, 5215–5221.

[17] B. Hinrichsen, R. E. Dinnebier, M. Jansen, *Z. Krist. Suppl. 23 (EPDIC IX proceeding)* **2006**, 231–236.

[18] a) S. I. Vagin, A. K. Ott, B. Rieger, *Chem. Ing. Technol.* **2007**, *79*, 767–780; b) Z. Wang, V. C. Kravtsov, R. B. Walsh, M. J. Zaworotko, *Cryst. Growth Des.* **2007**, *7*, 1154–1162; c) H. J. Park, M. P. Suh, *Chem. Eur. J.* **2008**, *14*, 8812–8821; d) B. Q. Ma, K. L. Mulfort, J. T. Hupp, *Inorg. Chem.* **2005**, *44*, 4912–4914; e) H. Chun, D. N. Dybtsev, H. Kim, K. Kim, *Chem. Eur. J.* **2005**, *11*, 3521–3529.

[19] A. A. García-Valdivia, A. Zabala-Lekuona, A. Goñi-Cárdenas, B. Fernández, J. A. García, J. F. Quílez del Moral, J. Cepeda, A. Rodríguez-Diéguez, *Inorg. Chim. Acta* **2020**, *509*, 119687.

[20] S. L. Griffin, C. Wilson, R. S. Forgan, *Front. Chem.* **2019**, *7*.

[21] a) A. Fateeva, P. Horcajada, T. Devic, C. Serre, J. Marrot, J. M. Grenèche, M. Morcrette, J. M. Tarascon, G. Maurin, G. Férey, *Eur. J. Inorg. Chem.* **2010**, *2010*, 3789–3794; b) D. Sun, S. Ma, J. M. Simmons, J.-R. Li, D. Yuan, H.-C. Zhou, *Chem. Commun.* **2010**, *46*, 1329–1331; c) V. Bon, I. Senkovska, I. A. Baburin, S. Kaskel, *Cryst. Growth Des.* **2013**, *13*, 1231–1237; d) N. Zhu, M. J. Lennox, T. Duren, W. Schmitt, *Chem. Commun.* **2014**, *50*, 4207–4210; e) G. Resnati, E. Boldyreva, P. Bombicz, M. Kawano, *IUCrJ* **2015**, *2*, 675–690; f) T. Tanasaro, K. Adpakpang, S. Ittisanronnachai, K. Faungnawakij, T. Butburee, S. Wannapaiboon, M. Ogawa, S. Bureekaew, *Cryst. Growth Des.* **2018**, *18*, 16–21; g) A.-X. Zhu, Q.-Y. Yang, A. Kumar, C. Crowley, S. Mukherjee, K.-J. Chen, S.-Q. Wang, D. O'Nolan, M. Shivanna, M. J. Zaworotko, *J. Am. Chem. Soc.* **2018**, *140*, 15572–15576; h) S.-J. Lee, J. L. Mancuso, K. N. Le, C. D. Malliakas, Y.-S. Bae, C. H. Hendon, T. Islamoglu, O. K. Farha, *ACS Mater. Lett.* **2020**, 499–504.

[22] C. Serre, F. Millange, C. Thouvenot, M. Noguès, G. Marsolier, D. Louër, G. Férey, *J. Am. Chem. Soc.* **2002**, *124*, 13519–13526.

[23] a) S. E. Henkelis, D. Rademacher, D. J. Vogel, N. R. Valdez, M. A. Rodriguez, L. E. S. Rohwer, T. M. Nenoff, *ACS Appl. Mater. Interfaces* **2020**, *12*, 22845–22852; b) S. E. Henkelis, D. L. Huber, D. J. Vogel, J. M. Rimsza, T. M. Nenoff, *ACS Appl. Mater. Interfaces* **2020**, *12*, 19504–19510; c) D. F. Sava Gallis, D. J. Vogel, G. A. Vincent, J. M. Rimsza, T. M. Nenoff, *ACS Appl. Mater. Interfaces* **2019**, *11*, 43270–43277.

Received: July 23, 2020

Journal of Inorganic and General Chemistry
ZAAC
Zeitschrift für anorganische und allgemeine Chemie

ARTICLE